

Computational prediction of samarium hydride at megabar pressure

Zelong Zhao,¹ Siyu Chen,² Bartomeu Monserrat,^{2,3} Evgeny Plekhanov,^{1,*} and Cedric Weber^{1,†}

¹*Theory and Simulation of Condensed Matter(TSCM),
King's College London, The Strand,London WC2R 2LS,UK*
²*TCM Group, Cavendish Laboratory, University of Cambridge,
J. J. Thomson Avenue, Cambridge CB3 0HE, United Kingdom*

³*Department of Materials Science and Metallurgy, University of Cambridge,
27 Charles Babbage Road, Cambridge CB3 0FS, United Kingdom*

Samarium hydrides, belonging to the broad class of lanthanide polyhydrides, have yet to be experimentally tested at high pressure. In this study, we use random structure searches to explore multiple possible stoichiometries and propose SmH_2 with a layered hexagonal structure in the $P6/mmm$ space group and SmH_6 with hydrogen clathrate structures in the Im-3m space group as theoretically stable phases of samarium hydrides at a wide range of pressures centered around 200 GPa. We further combine the first-principles methods of density functional theory and dynamical mean-field theory to explore many-body correlations in samarium hydrides, reporting electron and phonon dispersions and densities of states, and also evaluate the electron-phonon driven superconductivity to investigate low critical temperatures at 200 GPa.

I. INTRODUCTION

Superconductivity was first observed in the early 20th century at very low temperatures. Since then scientists have embarked on a long-standing quest towards finding materials with high critical temperatures T_c for practical use. The discovery of so-called high- T_c materials, starting with the copper oxides in the 1980s, has driven a revival of interest in the search for room temperature superconductors. Two mechanisms have been suggested to account for superconductivity: (i) the early proposal of Bardeen-Cooper-Schrieffer [1] in which electrons pair via phonon-mediated interactions, which accounts for type-I superconductors, and (ii) spin fluctuations, which account for the type-II high- T_c materials.

Ashcroft suggested that type-I superconductors could achieve a high T_c provided that the electron-phonon coupling strength was large [2]. The initial suggestion was to use high pressure metallic hydrogen [2], predicted to have a T_c higher than room temperature [3]. However, the pressure required to metallize hydrogen exceeds 400 GPa, which makes experiments extremely challenging [4]. Ashcroft later suggested that combining hydrogen with other elements would provide additional chemical pressure [5], resulting in a reduction of the metallization pressure while maintaining favorable phonon and electron-phonon coupling strengths. As a result, a variety of high pressure hydrides have been suggested to promote metallicity and superconductivity at experimentally viable pressures [6–10].

There are a large number of possible candidates for high pressure hydrides, with a wide range of chemical compositions and different stoichiometries, symmetries, and lattice structures. Computational studies [11, 12]

have predicted multiple candidates for such high- T_c hydride superconductors, and several experimental observations have also been reported. Importantly, these studies confirmed that superconductivity in several hydrides is phonon-mediated.[6].

Of the possible high pressure hydrides, contemporary studies focused on lanthanum hydrides [6] due to its high T_c of about 250 K at 170 GPa. This accessible pressure range motivated studies of many other lanthanide hydrides [13], both experimentally [6] and computationally [14, 15]. Despite these advances, a key lanthanide hydride, namely samarium hydride, has so far received little attention. Experimentally, samarium hydride has only been studied at ambient pressure [16], while computational studies of samarium hydride under high pressure are still lacking.

Crystal structure prediction methods[17–19] have been tremendously successful at identifying the stable phases of high pressure compounds. In these methods, first-principles calculations, typically using density functional theory (DFT), are performed across a wide range of candidate structures and compositions, and the best candidate materials are those with the lowest enthalpy.

Recent experiments have reported the high pressure phase diagram of samarium [20], which provides a solid platform on which to study samarium hydrides. In this study, we use *ab initio* random structure search (AIRSS) methodology [19, 21] together with DFT as implemented in the plane wave code CASTEP [22] to predict candidate structures for samarium-hydrogen compounds. The accuracy of the enthalpy determined for each generated structure depends on the quantum solver used, and we use DFT+U [23] to describe the local correlations in Sm. We find a number of possible candidates of Sm_yH_x , with $x = 1 \sim 18$ and $y = 1 \sim 2$ and under external pressures ranging from 1 to 400 GPa, as summarized in Fig. A1. SmH_2 in the $P6/mmm$ and SmH_6 in the Im-3m are identified as stable structures for 200 GPa. We also study the electronic and phononic properties and potential super-

* evgeny.plekhanov@kcl.ac.uk

† cedric.weber@kcl.ac.uk

conductivity of SmH₂ at 200 GPa. We find that SmH₂ has a very low critical superconducting critical temperature (T_c) below 1 K. and SmH₆ has a relatively higher T_c above 15 K.

Additionally, the electronic structure of this compound is studied with the state-of-the-art DFT+DMFT method, which provides an accurate description of strongly correlated electrons.

II. METHOD

A. Theory

1. Electronic structure methods

Within DFT [24, 25] the many-body Schrödinger equation is solved by mapping the problem onto an auxiliary one-body problem with the same electronic density as the many-body system. This auxiliary Kohn-Sham (KS) system obeys:

$$\left[-\frac{\hbar^2}{2m}\nabla^2 + V_{\text{eff}}(\mathbf{r}) \right] \varphi_i(\mathbf{r}) = \varepsilon_i \varphi_i(\mathbf{r}), \quad (1)$$

where the electrons experience an effective potential $V_{\text{eff}}(\mathbf{r})$:

$$V_{\text{eff}}(\mathbf{r}) = V_{\text{ext}}(\mathbf{r}) + \int \frac{n(\mathbf{r}')}{|\mathbf{r} - \mathbf{r}'|} d^3\mathbf{r}' + V_{\text{XC}}[n(\mathbf{r})]. \quad (2)$$

In these equations, $\varphi_i(\mathbf{r})$ is the i -th KS orbital, and the electronic density $n(\mathbf{r})$ is derived from the densities of the KS orbitals occupied up to the Fermi level. The accuracy of the KS scheme depends on the choice of exchange correlation (XC) functional. Commonly used approximations include the Local Density Approximation (LDA) and Generalized Gradient Approximations (GGA). In this work, we adopt the Perdew-Burke-Ernzerhof (PBE) XC functional [26], which is a type of GGA.

The amount of correlations contained in the DFT XC functional is not sufficient to treat the strong Coulomb repulsion in partially filled d and f orbitals. Within standard approximations to DFT functionals, these strongly correlated orbitals appear to be excessively delocalized. This lack of localization can be, to some extent, corrected with the DFT+U scheme, where the DFT energy functional is combined with an additional term proportional to a parameter, called Hubbard U , which penalizes the configurations with doubly occupied orbitals [27].

A higher level treatment of the strong Coulomb repulsion is provided by the DFT + Dynamical Mean Field Theory (DFT+DMFT) approach [28–30], where the temporal correlations are taken into account exactly, while the treatment of the spatial correlations becomes exact in the limit of infinite coordination of the correlated orbitals. Within DFT+DMFT, the system of correlated orbitals (usually d or f , or a subset of them) connected to a chemical environment is mapped onto an auxiliary

problem of an Anderson impurity connected to a bath of uncorrelated orbitals. The latter problem is then solved either numerically (e.g. quantum Monte Carlo, exact diagonalization) or analytically by using some approximation (e.g. Hubbard-I, auxiliary bosons). The results of such an impurity problem are then mapped back onto the original correlated lattice problem. The details of the DFT+DMFT implementation used in the present work can be found in Refs. 30 and 31.

2. Structure searching

We perform structure searches using AIRSS [19, 21] together with the DFT+U methodology. The efficiency of the structure search is crucial for searching low enthalpy compounds, and we adopt several strategies to accelerate calculations, including the adjustment of the volume and the use of low-resolution calculations during the initial potential energy surface scan, followed by higher-precision calculations. To obtain the convex hull of samarium hydride, we calculate the enthalpy of formation with:

$$\text{Sm}_y\text{H}_x = x \text{H} + y \text{Sm}. \quad (3)$$

This formula requires the knowledge of stable phases of the end members samarium [20] and hydrogen [32] atoms, which we take from the literature. For example, at 200 GPa, hydrogen is in a phase of $C2/c$ structure and samarium is in the $oF8$ phase.

We explain that the formation enthalpies found by this method are likely to overestimate the true formation enthalpies due to the oversimplified reaction pathway. We also highlight that it is generally impossible to confirm whether the global enthalpy minimum has been found due to the exponential scaling cost of searching over the potential energy landscape. However, structure searching methods generally provide important insights into high pressure phases.

B. Computational details

In the present work, we have performed the first principles calculations using the CASTEP and QUANTUM ESPRESSO codes. The GGA in the Perdew-Burke-Ernzerhof (PBE) variant and ultrasoft pseudopotentials (USPP) for Sm [Xe]4f⁶6s² and H 1s¹ were used for all DFT calculations.

The random structure search over Sm_yH_x stoichiometry was performed combining AIRSS [19] and CASTEP [22]. DFT+U calculations were carried out with $U = 3$ eV and 6 eV, and the spin polarized geometry optimization was done starting from the results of the random structure search. A two-step approach was adopted in order to facilitate the random structure search: in step (1)

the exploration of different stoichiometries with a coarse Monkhorst-Pack (MP) \mathbf{k} -point grid ($2\pi \times 0.03 \text{ \AA}^{-1}$), a kinetic energy cut-off of $E_{\text{cut}} = 500 \text{ eV}$, and a force tolerance of 0.05 eV/\AA , $U = 3 \text{ eV}$; and in step (2) on a smaller subset of structures having the lowest enthalpy within each symmetry group, the calculations with finer parameter set were run with a denser MP \mathbf{k} -point grid ($2\pi \times 0.01 \text{ \AA}^{-1}$), $E_{\text{cut}} = 600 \text{ eV}$, $U = 3 \text{ eV}$ and the force tolerance 0.001 eV/\AA . We note that the parameter set used in the second step ensures that the overall energy precision is within 1 meV/atom (see Fig. A3 Fig. A4).

For the most stable structure SmH_2 , we also performed DFT+DMFT calculations as implemented within CASTEP [22, 30, 31] using the same DFT parameters as the ones used in step (2) of the searches. Additionally, these calculations used a Hubbard $U = 6 \text{ eV}$ and an additional Hund's coupling $J = 0.855 \text{ eV}$.

The phonon dispersions were calculated in the harmonic approximation via the finite difference method [33] combined with nondiagonal supercells [34]. The coarse \mathbf{q} point grid for Brillouin zone sampling was $6 \times 6 \times 6$.

Electron-phonon coupling properties were calculated using density functional perturbation theory (DFPT) as implemented in the QUANTUM ESPRESSO package [35]. The coarse \mathbf{q} point grids used to sample the Brillouin zone were again of size $6 \times 6 \times 6$. The DFT settings involved in the DFPT calculation were identical to those used in step (2) of the searches. The superconducting critical temperature was found using the Allen and Dynes [36] revised McMillan [37] equation.

III. RESULT AND DISCUSSION

A. Structure Search

The random structure search was run a thousand times, and the results are summarized by the convex Hull as shown in Fig. 1. Each point corresponds to a distinct structure at a certain pressure and stoichiometry. In the convex Hull, the horizontal axis is the ratio x of hydrogen atoms relative to the total number of atoms in the cell in one formula unit (f.u.). The left side, corresponding to $x = 0$, is the samarium bulk, and the right side, corresponding to $x = 1$, is the hydrogen bulk. The solid line connects stable phases, while the dashed line connects the lowest enthalpy phases at each stoichiometry, which can be unstable.

Figure 1 indicates that a stable structure of the samarium-hydrogen system at high pressure has the stoichiometry SmH_2 in the space group $P6/mmm$. Interestingly, this structure is highly symmetric, a feature also observed in other high-pressure lanthanide hydride systems. The structure is analogous to the ScH_2 phase obtained in [15] for the scandium-hydrogen system. Furthermore, SmH_6 in the $Im-3m$ space group is analogous to YH_6 in [8].

Overall, the structures we have found tend to possess

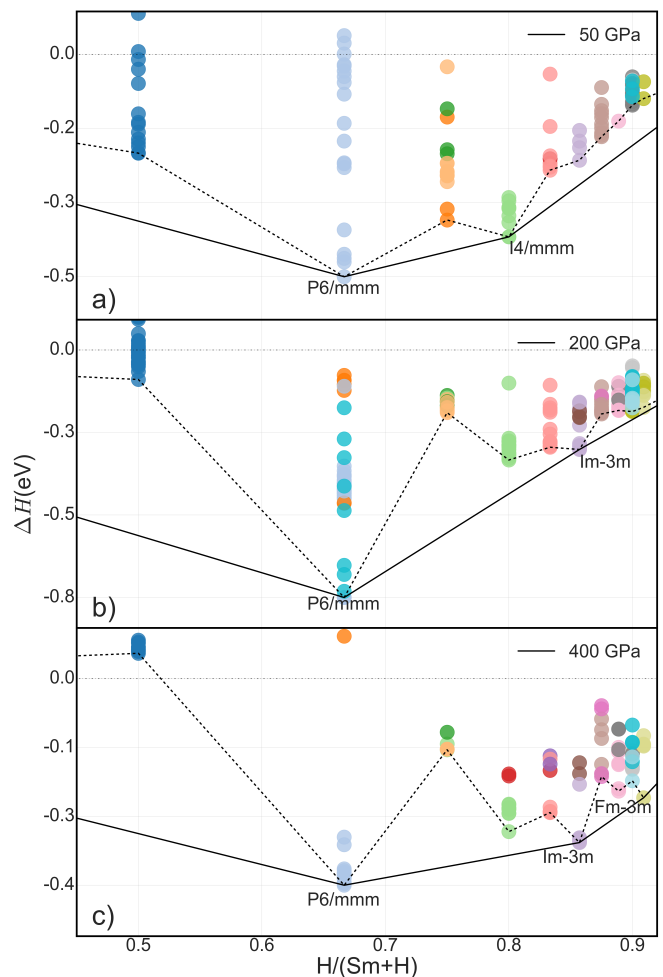


FIG. 1. Maxwell convex Hull reported at 50, 200, and 400 GPa. The solid line connects stable phases and the dashed line connects the lowest enthalpy phases at each stoichiometry (not necessarily stable). The end members are hydrogen in the $C2/c$ structure [32] and samarium in the $oF8$ phase [20].

a high symmetry at high pressure. It is important to note that the higher precision calculations on the most stable structures identified during the searches do not change the overall ranking of the low-enthalpy phases (see Fig. A2). Specifically, SmH_2 in the $P6/mmm$ space group remains the most stable phase.

We also remark that the enthalpies of elemental hydrogen and samarium enter the calculation of the formation energy. In this work, we use the theoretical estimates of solid hydrogen from Ref. [32], and the $oF8$ structure of samarium reported in Ref. [20]. Furthermore, our results remain unchanged upon a reasonable variation of the estimated hydrogen enthalpy, and in particular the order of the obtained phases remains the same in Fig. 1.

Between 50 GPa and 100 GPa, SmH_2 and SmH_4 (Fig. 2) are the most stable stoichiometries. SmH_2 exhibits a layered structure similar to MgB_2 . SmH_4 is $I4/mmm$ Ref. [15] is also been found as stable phase but at lower

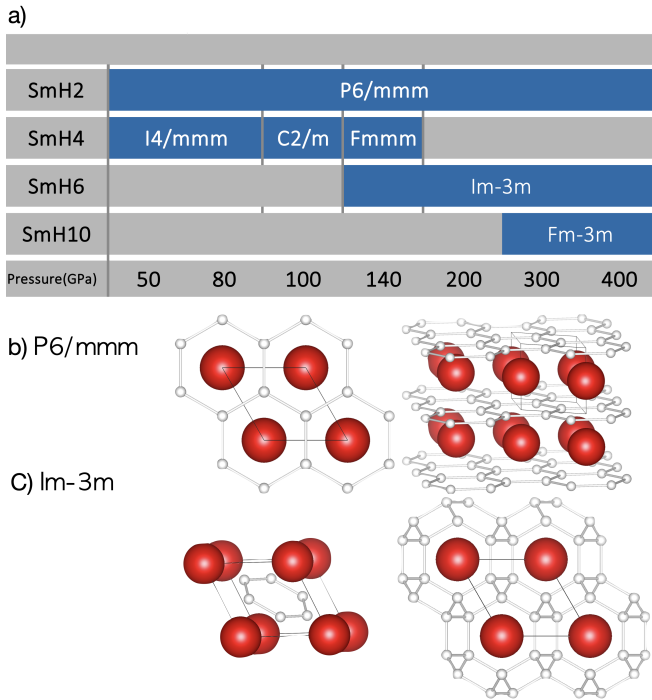


FIG. 2. (a) Stable phase of Sm. P6/mmm is a stable phase for all range of pressure. Other stable phase tends to have more hydrogen as pressure increases. (b) P6/mmm of SmH₂ and (c) Im-3m of SmH₆ at 200 GPa.

pressure.

SmH_x Convex Hull was previously reported in Ref. [15], where Sm replaced other elements in the hydrogen clathrate structure found. We have rediscovered the Im-3m, I4/mmm and Fm-3m structures by AIRSS combined with DFT+U. The contradiction of the convex hull structure between the current work and Ref. [15] is not only due to DFT settings, but also the P6/mmm phase exists in our work. Similarly, both results predict that phases containing even more hydrogen become competitive at higher pressures.

B. Electronic properties of SmH₂ P6/mmm and SmH₆ Im-3m

To investigate the electronic properties of SmH₂ of P6/mmm phase, we calculated the corresponding partial density of states (PDOS) in (Fig. 3). Only samarium contributes f-electrons, and TOT indicates the total DOS of SmH₂. The PBE exchange functional splits the DOS of the 4f electrons and causes steep negative slope at the Fermi level. The Hubbard U term in the DFT+U method includes the Mott transition via splitting the DOS of correlated orbitals and pushing the pseudo-particle peak away from the Fermi level. Both DFT+U with U (3 eV and 6 eV) predict the samarium 4f electrons peak away from the Fermi level.

To further capture the correlation effects of f-electrons,

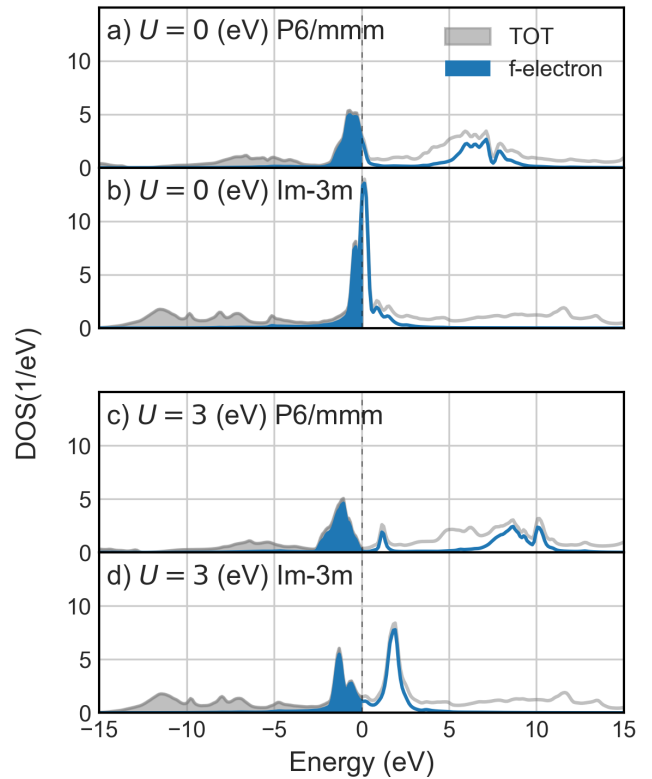


FIG. 3. DOS of SmH₂ P6/mmm predicted by (a) DFT with U= 0 eV and (c) DFT+U with U= 3 eV and Im-3m predicted by b) DFT with U= 0 eV and (d) DFT+U with U= 3 eV.

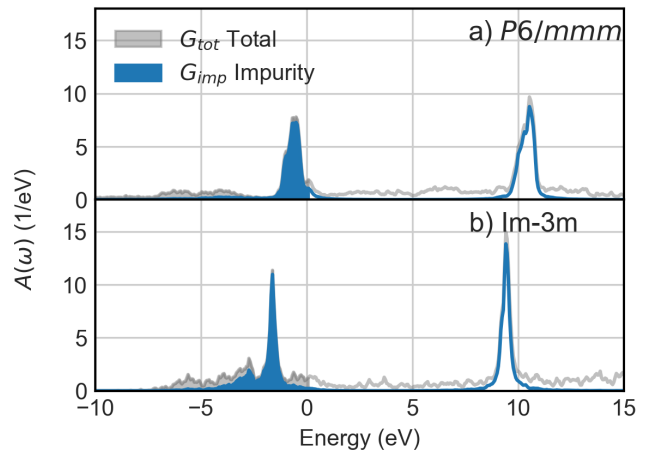


FIG. 4. DFT+DMFT density of state for P6/mmm and Im-3m at 200 GPa. Hubbard U, 6 eV. Hund's coupling J=0.85 eV.

we have performed DFT+DMFT calculations for SmH₂ P6/mmm and SmH₆ Im-3m at 200 GPa. We have used charge self-consistency (CSC) DFT+DMFT, which refers the convergence of the chemical potential involving in DMFT calculation and confirms that the charge number is consistent with the charge density. Our calcula-

tions show that the chemical potentials of DFT+U (Fig. 3) and DFT+DMFT (Fig. 4) show similar densities of states near the Fermi level.

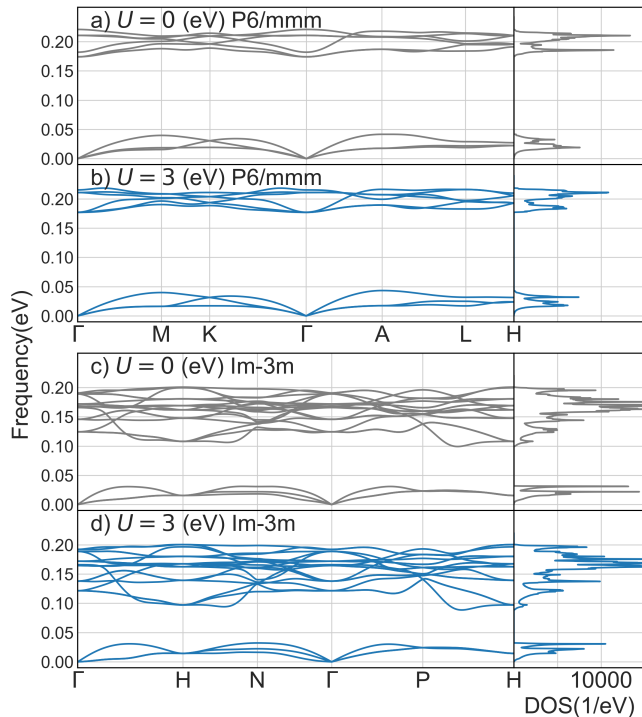


FIG. 5. The left side panel shows the SmH_2 in the $P6/mmm$ and SmH_6 in the Im-3m space group phonon dispersion and the right side panel shows the phonon DOS. Both are calculated with a coarse q-point grid size of $6 \times 6 \times 6$. Electronic method is DFT+U with U as indicated.

The phonon dispersion of SmH_2 in the $P6/mmm$ and SmH_6 in the Im-3m space group at 200 GPa using DFT and DFT+U exhibits no soft modes, which indicates that the predicted phase is dynamically stable. The phonons of samarium hydride show a similar pattern to those of other lanthanides hydrides. The most prominent feature is a large gap between optical and acoustic branches arising from the large difference in mass between lanthanides and hydrogen. Interestingly, the Hubbard U term has a negligible effect on the phonon dispersion. We also highlight that different values of U lead to an equilibrium volume for the $P6/mmm$ structure that varies from $15.72(\text{\AA})^3$ to $16.09(\text{\AA})^3$ for U between 0 eV and 3 eV and Im-3m structure that varies from $21.35(\text{\AA})^3$ to $22.45(\text{\AA})^3$. Given the negligible effect of the U value on the phonon frequencies, there is likely a competition between the volume changes and the effect of U on the force constants.

We further performed density functional perturbation theory (DFPT) calculations to estimate the electron-phonon coupling (EPC) strength and calculated the superconducting temperature (T_c) via the Allen and Dynes [36] revised McMillan [37] equation:

	λ	ω_{\log}	$T_c(K)$
$P6/mmm$	0.28	357.69	0.10 (K) ($\mu = 0.10$)
			0.00 (K) ($\mu = 0.15$)
Im-3m	0.65	900.04	26.35 (K) ($\mu = 0.10$)
			15.50 (K) ($\mu = 0.15$)

$$T_c = \frac{\omega_{\log}}{1.2} \exp \left[\frac{-1.04(1 + \lambda)}{\lambda(1 - 0.62\mu^*) - \mu^*} \right] \quad (4)$$

Here, μ^* is the Coulomb potential with typical values between 0.1 to 0.15. λ is the electron-phonon coupling strength. ω_{\log} is the logarithmic average frequency. These quantities are evaluated via integrals of the Eliashberg function:

Electron-phonon coupling of SmH_2 $P6/mmm$ is relatively low at 0.28 and thus T_c is less than 1 K for μ^* between 0.1 and 0.15. As Im-3m has a relatively higher peak at Fermi level, the predicted T_c is relatively higher also. This result is consistent with earlier work [15, 38], which shows higher T_c for La/Y hydrides and lower T_c for intermediate series lanthanides such as Sm. The origin of the low T_c in samarium hydride could be caused by low hydrogen DOS at the Fermi level and the associated weak electron-phonon coupling strength.

In conclusion, we used random structure searches via the AIRSS method [19, 21, 32] to explore high pressure samarium hydride, a material whose structure remains unknown experimentally at high pressures. Focusing on a pressure of 200 GPa, we predicted that SmH_2 with a structure of $P6/mmm$ symmetry is the most stable phase. Meta-stable phases are found for SmH_y for y equal to 4, 6, and 10. These results indicate that high pressure samarium hydride compounds could be hydrogen-rich. We then systematically studied the electronic structure and lattice dynamics of SmH_2 , finding that SmH_2 is dynamically stable for all studied values of U between 0 and 6 eV. Finally, we find that the superconducting critical temperature T_c is less than 1 K.

This work opens new avenues for studying hydrides at high pressure. As shown in this work, new highly symmetric phases of correlated matter can emerge, leading to a breadth of properties which are interesting for possible applications, such as superconductivity. The method used in this work is quite general and can be extended to other systems of interest.

ACKNOWLEDGEMENTS

C.W. and E.P. are supported by the grant [EP/R02992X/1] from the UK Engineering and Physical Sciences Research Council (EPSRC). S.C. acknowledges financial support from the Cambridge Trust and

from the Winton Programme for the Physics of Sustainability. B.M. acknowledges support from a UKRI Future Leaders Fellowship (Grant No. MR/V023926/1), from the Gianna Angelopoulos Programme for Science, Technology, and Innovation, and from the Winton Programme for the Physics of Sustainability. This work was performed using resources provided by the ARCHER

UK National Supercomputing Service and the Cambridge Service for Data Driven Discovery (CSD3) operated by the University of Cambridge Research Computing Service (www.csd3.cam.ac.uk), provided by Dell EMC and Intel using Tier-2 funding from the Engineering and Physical Sciences Research Council (capital grant EP/P020259/1), and DiRAC funding from the Science and Technology Facilities Council (www.dirac.ac.uk).

-
- [1] J. Bardeen, L. N. Cooper, and J. R. Schrieffer, *Physical review* **108**, 1175 (1957).
- [2] N. W. Ashcroft, *Physical Review Letters* **21**, 1748 (1968).
- [3] J. M. McMahon and D. M. Ceperley, *Physical Review B* **84**, 144515 (2011).
- [4] R. P. Dias and I. F. Silvera, *Science* **355**, 715 (2017).
- [5] N. Ashcroft, *Physical Review Letters* **92**, 187002 (2004).
- [6] M. Somayazulu, M. Ahart, A. K. Mishra, Z. M. Geballe, M. Baldini, Y. Meng, V. V. Struzhkin, and R. J. Hemley, *Physical Review Letters* **122**, 027001 (2019).
- [7] Y. Sun, J. Lv, Y. Xie, H. Liu, and Y. Ma, *Physical review letters* **123**, 097001 (2019).
- [8] P. Kong, V. S. Minkov, M. A. Kuzovnikov, A. P. Drozdov, S. P. Besedin, S. Mozaffari, L. Balicas, F. F. Balakirev, V. B. Prakapenka, S. Chariton, *et al.*, *Nature communications* **12**, 1 (2021).
- [9] D. Zhou, D. V. Semenok, D. Duan, H. Xie, W. Chen, X. Huang, X. Li, B. Liu, A. R. Oganov, and T. Cui, *Science advances* **6**, eaax6849 (2020).
- [10] C. Heil, S. Di Cataldo, G. B. Bachelet, and L. Boeri, *Physical Review B* **99**, 220502 (2019).
- [11] D. C. Lonie, J. Hooper, B. Altintas, and E. Zurek, *Physical Review B* **87**, 054107 (2013).
- [12] Y. Li, J. Hao, H. Liu, Y. Li, and Y. Ma, *The Journal of chemical physics* **140**, 174712 (2014).
- [13] Y. Fukai, *The metal-hydrogen system: basic bulk properties*, Vol. 21 (Springer Science & Business Media, 2006).
- [14] E. Plekhanov, Z. Zhao, F. Macheda, Y. Wei, N. Bonini, and C. Weber, *Physical Review Research* **4**, 013248 (2022).
- [15] F. Peng, Y. Sun, C. J. Pickard, R. J. Needs, Q. Wu, and Y. Ma, *Physical review letters* **119**, 107001 (2017).
- [16] J. Daou, P. Vajda, and J. Burger, *Solid state communications* **71**, 1145 (1989).
- [17] C. W. Glass, A. R. Oganov, and N. Hansen, *Computer physics communications* **175**, 713 (2006).
- [18] Y. Wang, J. Lv, L. Zhu, and Y. Ma, *Computer Physics Communications* **183**, 2063 (2012).
- [19] C. J. Pickard and R. Needs, *Journal of Physics: Condensed Matter* **23**, 053201 (2011).
- [20] S. Finnegan, E. Pace, C. Storm, M. McMahon, S. MacLeod, H.-P. Liermann, and K. Glazyrin, *Physical Review B* **101**, 174109 (2020).
- [21] C. J. Pickard and R. Needs, *Physical Review Letters* **97**, 045504 (2006).
- [22] S. J. Clark, M. D. Segall, C. J. Pickard, P. J. Hasnip, M. I. Probert, K. Refson, and M. C. Payne, *Zeitschrift für kristallographie-crystalline materials* **220**, 567 (2005).
- [23] M. Cococcioni, *Correlated Electrons: From Models to Materials Modeling and Simulation* **2** (2012).
- [24] W. Kohn and L. J. Sham, *Physical review* **140**, A1133 (1965).
- [25] P. Hohenberg and W. Kohn, *Physical review* **136**, B864 (1964).
- [26] J. P. Perdew, K. Burke, and M. Ernzerhof, *Physical review letters* **77**, 3865 (1996).
- [27] B. Himmetoglu, A. Floris, S. De Gironcoli, and M. Cococcioni, *International Journal of Quantum Chemistry* **114**, 14 (2014).
- [28] A. Georges, G. Kotliar, W. Krauth, and M. J. Rozenberg, *Reviews of Modern Physics* **68**, 13 (1996).
- [29] G. Kotliar, S. Y. Savrasov, K. Haule, V. S. Oudovenko, O. Parcollet, and C. Marianetti, *Reviews of Modern Physics* **78**, 865 (2006).
- [30] E. Plekhanov, P. Hasnip, V. Sacksteder, M. Probert, S. J. Clark, K. Refson, and C. Weber, *Physical Review B* **98**, 075129 (2018).
- [31] E. Plekhanov, N. Bonini, and C. Weber, *Phys. Rev. B* **104**, 235131 (2021).
- [32] C. J. Pickard and R. J. Needs, *Nature Physics* **3**, 473 (2007).
- [33] K. Parlinski, Z. Q. Li, and Y. Kawazoe, *Phys. Rev. Lett.* **78**, 4063 (1997).
- [34] J. H. Lloyd-Williams and B. Monserrat, *Phys. Rev. B* **92**, 184301 (2015).
- [35] P. Giannozzi, S. Baroni, N. Bonini, M. Calandra, R. Car, C. Cavazzoni, D. Ceresoli, G. L. Chiarotti, M. Cococcioni, I. Dabo, *et al.*, *Journal of physics: Condensed matter* **21**, 395502 (2009).
- [36] P. B. Allen and R. Dynes, *Physical Review B* **12**, 905 (1975).
- [37] W. McMillan, *Physical Review* **167**, 331 (1968).
- [38] D. V. Semenok, I. A. Kruglov, I. A. Savkin, A. G. Kvashnin, and A. R. Oganov, *Current Opinion in Solid State and Materials Science* **24**, 100808 (2020).

Supplemental Materials: Computational prediction of Samarium Hydride at Mgebar pressure

I. RANDOM STRUCTURE SEARCH

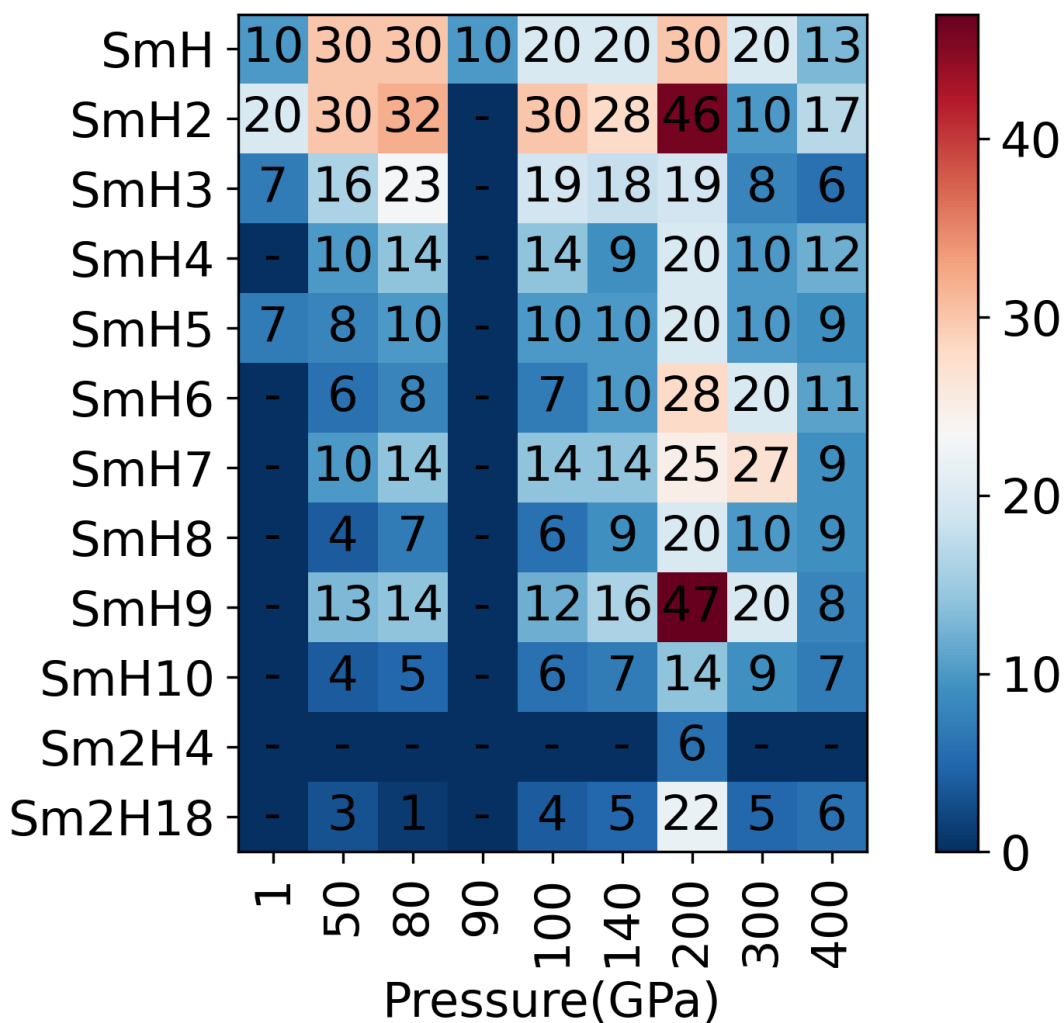


FIG. A1. Size of the phase database. Y-axis is stoichiometry of Samarium and hydrogen. X-axis is pressure we performed random structure search. Phase we searched "-" represents we did not search for this pressure and stoichiometry. The number indicated in each of the cell is the total number of distinct structure identified by AIRSS at each pressure for each stoichiometry. Colour bar blue for less search performed for this combination and red represents for more intense search.

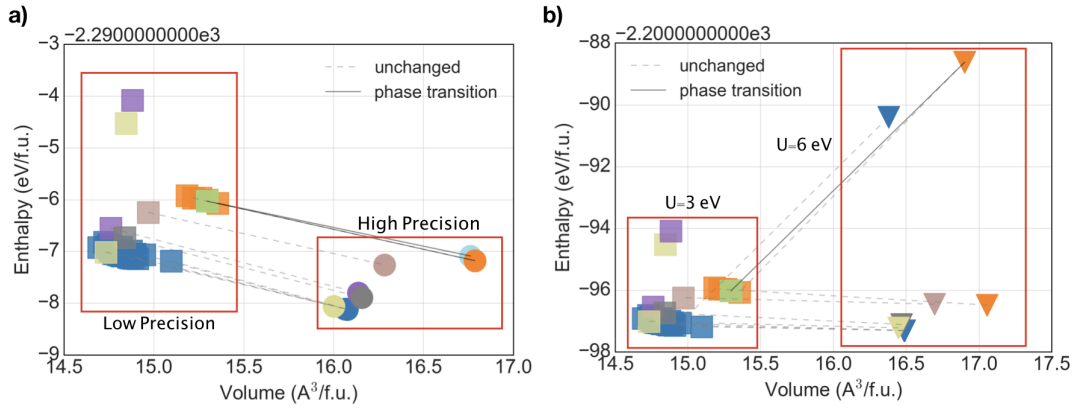


FIG. A2. AIRSS generated phases of SmH_2 at 200 GPa. Squares and circles indicate phases of SmH_2 . Color indicates space group. Square indicate relevant DFT+U settings is "step 1" as mentioned in the main paper and circles represent "step 2". X axis is volume of the unit cell and Y axis is DFT+U calculated enthalpy. Phases in both "Low Precision and (b) "U=3eV" boxes are same group of phases and DFT+U settings are indicated are "step 1" in the method section. (a) DFT settings changed between "Low Precision" ("step 1") to "High Precision" ("step 2") but Hubbard U is kept same. (b) DFT settings changed as in (a) but Hubbard U involved in DFT+U calculation changed from 3 eV to 6 eV.

TABLE A1. Lattice parameters of Sm_xH_y

	Space group	Lattice Parameters Å	Atom	Atomic fractional coordinates		
				X	Y	Z
SmH_2 (200 GPa)	$P6/mmm$	$a=b=2.691931$	Sm(1b)	0.00000	0.00000	0.00000
		$c=2.561747$	H(2c)	1/3	2/3	1/2
		$\alpha = \beta = \gamma = 90^\circ$				
		$\gamma = 120^\circ$				
SmH_4 (200 GPa)	$I4/mmm$	$a=b=2.54632297$	Sm(2b)	0.00000	0.00000	1/2
		$c=5.61849941$	H(4e)	1/2	1/2	0.69300
		$\alpha = \beta = \gamma = 90^\circ$	H(4d)	0.00000	1/2	3/4
SmH_4 (100 GPa)	$C2/m$	$a=5.552658$	Sm(2a)	1/2	1/2	0.00000
		$b=2.841566$	H(4i)	0.90102	1/2	0.45450
		$c=3.040550$	H(4i)	0.74689	1/2	0.66851
		$\alpha = \gamma 90^\circ$				
SmH_4 (140 GPa)	$Fmmm$	$\beta = 112.492036^\circ$				
		$a=3.7920738$	Sm(4b)	0.00000	0.00000	1/2
		$b=4.141084$	H(8f)	3/4	3/4	3/4
		$c=5.238472$	H(8i)	1/2	1/2	0.07342
SmH_6 (140 GPa)	$Im-3m$	$\alpha = \beta = \gamma = 90^\circ$	Sm(2a)	1/2	1/2	1/2
			H(12d)	1/2	1/4	0.00000
SmH_{10} (400 GPa)	$Fm-3m$	$a=b=c=4.43446568$	Sm(4a)	1/2	0.00000	1/2
		$\alpha = \beta = \gamma = 90^\circ$	H(8c)	3/4	1/4	1/4
			H(32f)	0.62044	0.62044	0.37956

II. DFT+DMFT CALIBRATION

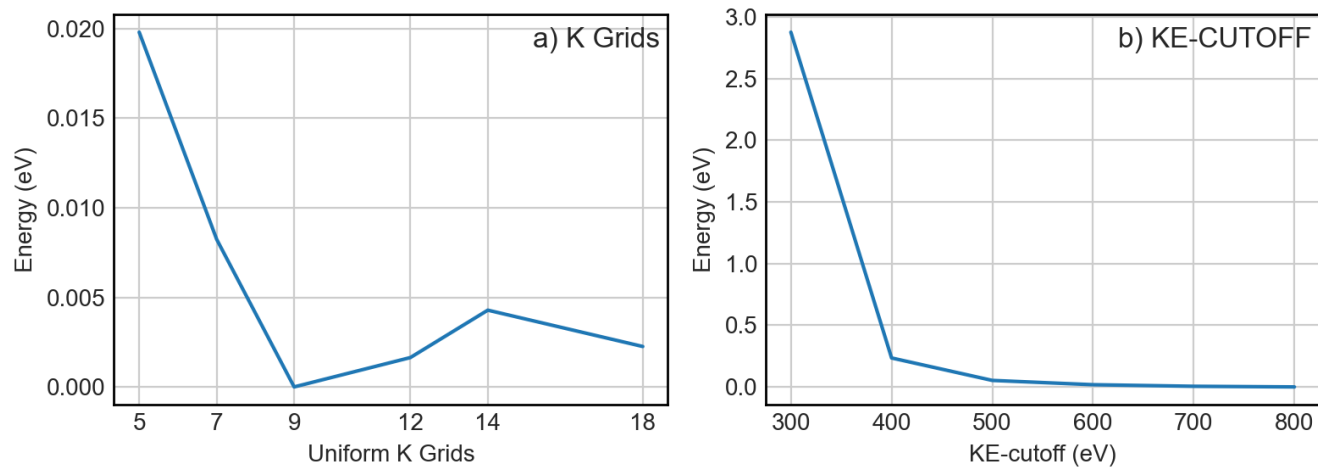


FIG. A3. DFT Convergence test of P6/mmm: a) K-points test. KE-cutoff 400eV with XC functional PBE. b) KE cut-off test with K-points grids 14 14 14 and XC functional PBE.

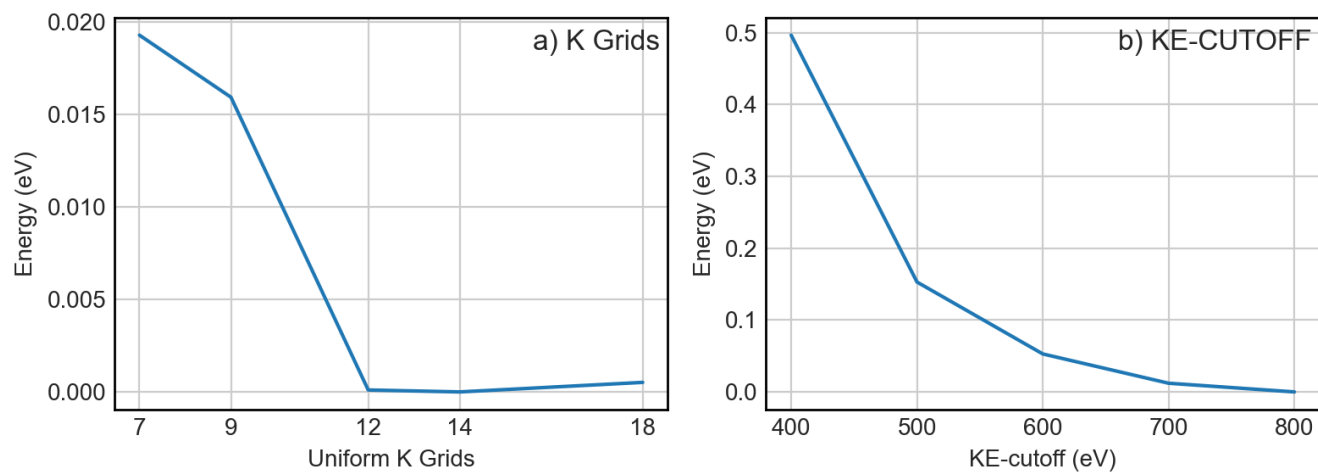


FIG. A4. DFT Convergence test of Im-3m: a) K Grids test. KE-cutoff 400eV with XC functional PBE. b) KE cut-off test with K-points grids 14 14 14 and XC functional PBE.

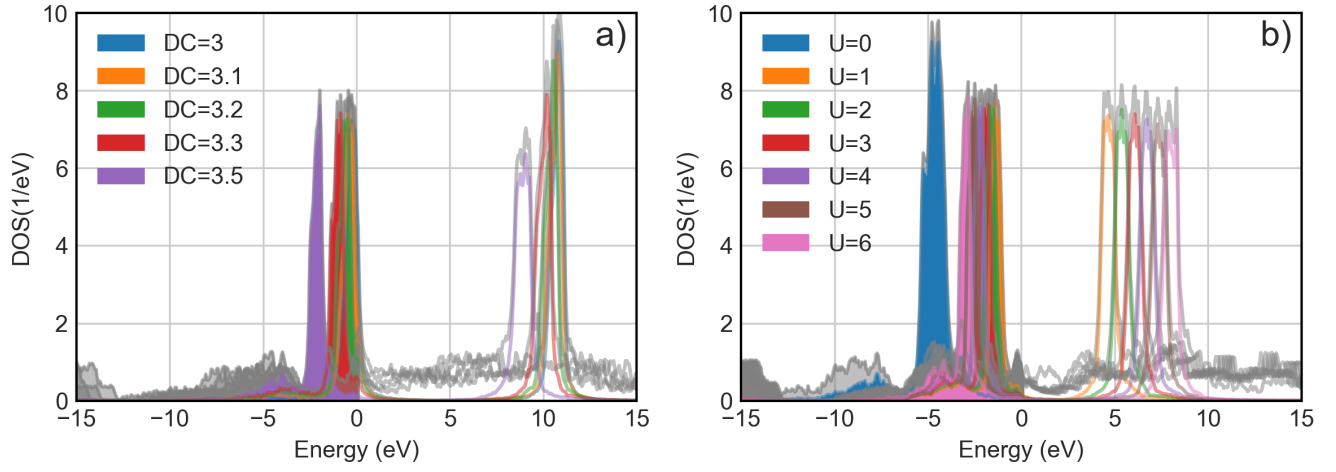


FIG. A5. (a) DC test with DFT+DMFT CSC DOS for $P6/mmm$ SmH_2 : Hubbard U equal to 6eV and Hund's coupling J equal to 0.855eV (b) Hubbard U test with 1-shot DOS for $P6/mmm$ SmH_2 : DC 3.5 and Hund's coupling J 0.855. Notice that Converged DC for $P6/mmm$ is around 3.1